Spectral Methods - Part 2: A comparative study of reduced order models for moisture transfer diffusive problems

Suelen Gasparin, Julien Berger, Denys Dutykh, Nathan Mendes

Suelen Gasparin
Pontifical Catholic University of Paraná, Brazil
LAMA–CNRS, Université Savoie Mont Blanc, France

Julien Berger
LOCIE–CNRS, Université Savoie Mont Blanc, France

Denys Dutykh
LAMA–CNRS, Université Savoie Mont Blanc, France

Nathan Mendes
Pontifical Catholic University of Paraná, Brazil

Spectral Methods – Part 2: A comparative study of reduced order models for moisture transfer diffusive problems

arXiv.org / HAL

Last modified: May 14, 2017

Spectral Methods — Part 2: A comparative study of reduced order models for moisture transfer diffusive problems

Suelen Gasparin*, Julien Berger, Denys Dutykh, and Nathan Mendes

Abstract. This paper explores in details the capabilities of two model reduction techniques – the Spectral Reduced Order Model (Spectral–ROM) and the Proper Generalised Decomposition (PGD) – to numerically solve moisture diffusion problems. Both techniques assume separated tensorial representation of the solution by a finite sum of function products. The Spectral–ROM fixes a set of spatial basis functions to be the Chebyshev polynomials and then, a system of ordinary differential equations is built to compute the temporal coefficients of the solution using the Galerkin projection method, while the PGD aims at computing directly the basis of functions by minimising the residual. Both approaches are compared for three different cases: i) linear transfer; ii) parametric problems and iii) nonlinear diffusive transfer. Results have highlighted that both numerical techniques provide accurate solution and enable to reduce significantly the order of the model, allowing a fast computation of physical phenomena such as the moisture buffer effects that occur in porous building materials. For the linear and nonlinear cases, the Spectral–ROM error decreases faster than the one for the PGD. Moreover, fewer modes are required for the Spectral to compute a solution with equivalent accuracy. However, for the parametric case, the PGD computed a reduced order model whose outputs depend not only on the coordinates of space and time x and t, but also on the coordinate of the parameter belonging to a defined interval. On the other hand, the outputs of the Spectral–ROM depend only on the coordinates of space and time. The solution of the parametric problem is obtained by computing the solution for each numerical value of a given parameter within the defined interval.

Key words and phrases: reduced-order modelling; moisture diffusion; numerical methods; spectral methods; Proper Generalised Decomposition (PGD)

MSC: [2010] 35R30 (primary), 35K05, 80A20, 65M32 (secondary)
PACS: [2010] 44.05.+e (primary), 44.10.+i, 02.60.Cb, 02.70.Bf (secondary)

Key words and phrases. reduced-order modelling; moisture diffusion; numerical methods; spectral methods; Proper Generalised Decomposition (PGD).

* Corresponding author.

Contents

1. Introduction

Moisture in buildings is a subject of major concern as it may affect the energy consumption and demand, besides its impact on the building occupants' health and on material durability as well. For the assessment of moisture effects, numerical tools have been developed to accurately simulate the processes of heat and moisture transfer in buildings. Some successful applications of hygrothermal prediction tools are presented in [58].

Those tools are built using numerical approaches and discrete representations of the continuous equations by means of standard and incremental techniques to compute the solution. Due to stability conditions, most of the approaches are based on implicit schemes as described in [10, 27, 35, 36, 41, 54, 56]. Nevertheless, these schemes require the solution of large systems of equations (an order of 10^6 for 3−dimensional problems). Moreover, when considering nonlinear building material properties, sub-iterations at each time step are induced, increasing significantly the computational cost as mentioned in [1, 23, 24, 42]. Thus, innovative and efficient ways of numerical simulation are worth of further investigation.

Recently, in [29], the improved explicit Dufort–Frankel scheme was explored for the solution of moisture diffusion equation highlighting that the standard stability limitation can be overcome. Considering a nonlinear case of moisture transfer, it was reported that the proposed explicit approach needed only 15 % of the CPU time required by the Crank–Nicolson scheme to compute the solution. Even if numerical gains are observed, these approaches are still based on large original models, whose complexity is of order of $p \sim \mathcal{O}(10^6)$ or even $p \sim \mathcal{O}(10^7)$, in which p is the number of operations of the model. For this reason, model reduction techniques appear as a very interesting alternative to substantially reduce the number of operations and save computational resources (CPU time and memory).

Model reduction techniques aim at decreasing the model *order*, preserving a satisfactory accuracy to represent the physical phenomena. In building physics, several model reduction techniques have been employed. The *a posteriori* approaches have been used such as Proper Orthogonal Decomposition (POD) for linear heat and moisture transfer in [48] or Modal Basis Reduction (MBR) for convective heat transfer problems in [31, 32, 49]. *A priori* techniques such as Proper Generalized Decomposition (PGD) have been used in [13] to treat nonlinear heat and moisture transfer problems. More recently, the *a priori* Spectral Reduced Order Model has also presented interesting results in [28]. Therefore, this paper aims at comparing these two *a priori* reduced order model techniques, to compute the moisture diffusive transfer in porous materials. The *a posteriori* methods are not considered here due to their inherent extra-computational cost. Several features of the methods are analyzed in terms of both model order reduction and accuracy of the computed solution. The investigation is carried for three case studies: (i) linear transfer; (ii) parametric problems, aiming at computing a model whose solution depends on the material properties and (iii) nonlinear transfer with moisture dependent material properties.

Therefore, the manuscript is organized as follows: first, Section 2 presents the description of the physical phenomena; then Section 3 gives explanation of the PGD and Spectral reduced order model techniques; and, further sections present the three different case studies: (i) linear transfer in Section 4; (ii) parametric problem in Section 5 and (iii) nonlinear transfer in Section 6.

2. Moisture transfer in porous materials

The physical problem involves unidimensional moisture diffusion through a porous material defined by the spatial domain $\Omega_x = [0, L]$. The moisture transfer only occurs according to the liquid and vapor diffusion. The physical problem can be formulated as [35]:

$$\frac{\partial \rho_{l+v}}{\partial t} = \frac{\partial}{\partial x}\left(k_l \frac{\partial P_c}{\partial x} + k_v \frac{\partial P_v}{\partial x} \right), \tag{2.1}$$

where ρ_{l+v} is the volumetric moisture content of the material and k_v and k_l are the vapor and liquid permeabilities.

Eq. (2.1) can be written using the vapor pressure P_v as the driving potential. For this, we consider the physical relation, known as the Kelvin equation, between P_v and P_c:

$$P_c = R_v \cdot T \cdot \ln\left(\frac{P_v}{P_s(T)}\right),$$
$$\frac{\partial P_c}{\partial P_v} = \frac{R_v T}{P_v}.$$

Thus, we have:

$$\frac{\partial P_c}{\partial x} = \frac{\partial P_c}{\partial P_v} \cdot \frac{\partial P_v}{\partial x} + \frac{\partial P_c}{\partial T} \cdot \frac{\partial T}{\partial x}.$$

As we consider the mass transfer under isothermal conditions, the second term vanishes and we obtain:

$$\frac{\partial P_c}{\partial x} = \frac{R_v T}{P_v} \cdot \frac{\partial P_v}{\partial x}.$$

In addition, we have:

$$\frac{\partial \rho_{l+v}}{\partial t} = \frac{\partial \rho_{l+v}}{\partial \phi} \cdot \frac{\partial \phi}{\partial P_v} \cdot \frac{\partial P_v}{\partial t} + \frac{\partial \rho_{l+v}}{\partial T} \cdot \frac{\partial T}{\partial t} \simeq \frac{\partial \rho_{l+v}}{\partial \phi} \cdot \frac{\partial \phi}{\partial P_v} \cdot \frac{\partial P_v}{\partial t}.$$

Considering the relation $\rho_{l+v} = f(\phi) = f(P_v, T)$, obtained from material properties and from the relation between the vapour pressure P_v and the relative humidity ϕ, we get:

$$\frac{\partial \rho_{l+v}}{\partial t} = f'(P_v) \frac{1}{P_s} \frac{\partial P_v}{\partial t}.$$

Eq. (2.1) can be therefore rewritten as:

$$f'(P_v) \cdot \frac{1}{P_s} \cdot \frac{\partial P_v}{\partial t} \;=\; \frac{\partial}{\partial x} \left[\left(k_l \, \frac{R_v T}{P_v} \;+\; k_v \right) \frac{\partial P_v}{\partial x} \right] . \tag{2.2}$$

The material properties f, k_l and k_v depend on the vapor pressure P_v. Therefore, we denote $d_m \overset{\text{def}}{:=} k_l \cdot \frac{R_v T}{P_v} + k_v$ as the global moisture transport coefficient and $c_m \overset{\text{def}}{:=} f'(P_v) \, \frac{1}{P_s}$ the moisture storage coefficient.

At the material bounding surfaces, ROBIN-type boundary conditions are considered:

$$\left(k_l \, \frac{R_v T}{P_v} \;+\; k_v \right) \cdot \frac{\partial P_v}{\partial x} \;=\; h_{v,\mathrm{L}} \cdot (P_v \;-\; P_{v,\mathrm{L}}) \;-\; g_{l,\mathrm{L}} \,, \qquad x \;=\; 0 \,, \tag{2.3a}$$

$$-\left(k_l \, \frac{R_v T}{P_v} \;+\; k_v \right) \cdot \frac{\partial P_v}{\partial x} \;=\; h_{v,\mathrm{R}} \cdot (P_v \;-\; P_{v,\mathrm{R}}) \;-\; g_{l,\mathrm{R}} \,, \qquad x \;=\; L \,, \tag{2.3b}$$

where $P_{v,\mathrm{L}}$ and $P_{v,\mathrm{R}}$ are the vapor pressure of the ambient air, $g_{l,\mathrm{L}}$ and $g_{l,\mathrm{R}}$ are the liquid flow (driving rain) at the two bounding surfaces. We consider a uniform vapor pressure distribution as the initial condition:

$$P_v \;=\; P_v^i \,, \qquad\qquad t \;=\; 0 \,.$$

It is important to obtain a unitless formulation of governing equations while performing mathematical and numerical analysis of given practical problems, due to a certain number of reasons already discussed in [29]. Therefore, we define the following dimensionless parameters:

$$u \;=\; \frac{P_v}{P_v^i} \,, \qquad u_{\mathrm{R}} \;=\; \frac{P_{v,\mathrm{R}}}{P_v^i} \,, \qquad u_{\mathrm{L}} \;=\; \frac{P_{v,\mathrm{L}}}{P_v^i} \,, \qquad x^\star \;=\; \frac{x}{L} \,,$$

$$t^\star \;=\; \frac{t}{t^0} \,, \qquad c_m^\star \;=\; \frac{c_m \cdot L^2}{d_m^0 \cdot t^0} \,, \qquad d_m^\star \;=\; \frac{d_m}{d_m^0} \,, \qquad \mathrm{Bi}_{v,\mathrm{L}} \;=\; \frac{h_{v,\mathrm{L}} \cdot L}{d_m^0} \,,$$

$$\mathrm{Bi}_{v,\mathrm{R}} \;=\; \frac{h_{v,\mathrm{R}} \cdot L}{d_m^0} \,, \qquad g_{l,\mathrm{L}}^\star \;=\; \frac{g_{l,\mathrm{L}} \cdot L}{d_m^0 \cdot P_v^i} \,, \qquad g_{l,\mathrm{R}}^\star \;=\; \frac{g_{l,\mathrm{R}} \cdot L}{d_m^0 \cdot P_v^i} \,.$$

In this way, the dimensionless governing equations are then written as:

$$c_m^\star \frac{\partial u}{\partial t^\star} \;=\; \frac{\partial}{\partial x^\star} \left(d_m^\star \, \frac{\partial u}{\partial x^\star} \right) , \qquad t^\star \;>\; 0 \,, \qquad x^\star \;\in\; \left[0, \, 1 \right] , \tag{2.4a}$$

$$d_m^\star \frac{\partial u}{\partial x^\star} \;=\; \mathrm{Bi}_{v,\mathrm{L}} \cdot (u \;-\; u_{\mathrm{L}}) \;-\; g_{l,\mathrm{L}}^\star \,, \qquad t^\star \;>\; 0 \,, \qquad x^\star \;=\; 0 \,, \tag{2.4b}$$

$$-\, d_m^\star \frac{\partial u}{\partial x^\star} \;=\; \mathrm{Bi}_{v,\mathrm{R}} \cdot (u \;-\; u_{\mathrm{R}}) \;-\; g_{l,\mathrm{R}}^\star \,, \qquad t^\star \;>\; 0 \,, \qquad x^\star \;=\; 1 \,, \tag{2.4c}$$

$$u \;=\; 1 \,, \qquad\qquad t^\star \;=\; 0 \,, \qquad x^\star \;\in\; \left[0, \, 1 \right] . \tag{2.4d}$$

Finally, this is the problem of interest considered in this work. The procedure of the methods used for the problem solution is described in the next section.

3. Methodology

For the sake of simplicity, without losing the generality, the methods are first explained considering $d_m^\star$ and $c_m^\star$ as constants, noting $\nu \overset{\text{def}}{:=} \dfrac{d_m^\star}{c_m^\star}$ and thus, considering a linear diffusion equation:

$$\frac{\partial u}{\partial t} = \boldsymbol{\nabla} \cdot \Big(\nu \, \boldsymbol{\nabla} u \Big) , \tag{3.1}$$

for $x \in \big[-1, 1 \big]$. The boundary conditions are:

$$\frac{\partial u}{\partial x} = \mathrm{Bi}_{v,\mathrm{L}} \Big(u - u_{\mathrm{L}}(t) \Big) , \qquad x = -1 , \tag{3.2a}$$

$$-\frac{\partial u}{\partial x} = \mathrm{Bi}_{v,\mathrm{R}} \Big(u - u_{\mathrm{R}}(t) \Big) , \qquad x = 1 . \tag{3.2b}$$

Using a standard discretization method, such as Euler or Crank–Nicolson, to compute the solution of Eq. (3.1) yields in computing a solution $u(x,t)$ for each point of the discretised spatial and time domains. The following is adopted: N_x and N_t, which stand for the number of elements according to the discretization of the space and time domains. Thus, the order of the so-called large original model is $p = N_x \cdot N_t$.

Model reduction aims at decreasing the degrees of freedom present in a numerical model. It aims at approximating the solution by a lower order model $N \ll p$ without reducing drastically the fidelity of the physical model. One of the features is to significantly decrease the computational resources space (CPU time and memory). The reduced Spectral and PGD methodologies are described in the next Section.

3.1. Reduced Spectral method

Spectral methods consider a global representation of the solution, which means the derivative at a certain spatial point depends on the solution of the entire domain and not only on its neighbors [16]. Besides, spectral methods consider a sum of polynomials that suit for the whole domain, almost like an analytical solution, providing a high approximation of the solution. Therefore, as its error decreases exponentially, it is possible to have the same accuracy of other methods but with a lower number of Galerkin modes, which makes this method memory minimizing, allowing to store and operate a lower number of degrees of freedom [57].

3.1.1 Application of the Spectral–ROM

The idea of the spectral method is to assume that the unknown $u(x,t)$ from Eq. (3.1) can be approximatively represented as a finite sum [40, Chapter 6]:

$$u(x,t) \approx u_n(x,t) = \sum_{i=0}^{n} a_i(t)\,\phi_i(x). \tag{3.3}$$

Here, $\{\phi_i(x)\}_{i=0}^{n}$ is a set of basis functions that remains constant in time, $\{a_i(t)\}_{i=0}^{n}$ are the corresponding time-dependent spectral coefficients, n represents the number of degrees of freedom of the solution. Eq. (3.3) can be seen as a series truncation after $N = n+1$ modes [28]. The Chebyshev polynomials are chosen as the basis functions as they are optimal in $\mathcal{L}_\infty$ approximation norm [30]. Therefore, we have:

$$\phi_i(x) \equiv T_i(x).$$

For more details on Chebyshev polynomials the readers may refer to [16, 50]. As we have chosen the basis functions, we can compute the derivatives:

$$\frac{\partial u_n}{\partial x} = \sum_{i=0}^{n} a_i(t)\frac{\partial T_i}{\partial x}(x) = \sum_{i=0}^{n} \tilde{a}_i(t)\,T_i(x), \tag{3.4a}$$

$$\frac{\partial^2 u_n}{\partial x^2} = \sum_{i=0}^{n} a_i(t)\frac{\partial^2 T_i}{\partial x^2}(x) = \sum_{i=0}^{n} \tilde{\tilde{a}}_i(t)\,T_i(x), \tag{3.4b}$$

$$\frac{\partial u_n}{\partial t} = \sum_{i=0}^{n} \dot{a}_i(t)\,T_i(x), \tag{3.4c}$$

where the dot denotes $\dot{a}_i(t) \overset{\text{def}}{:=} \dfrac{\mathrm{d}a(t)}{\mathrm{d}t}$. Note that the derivatives are re-expanded in the same Chebyshev basis function. As a result, coefficients $\{\tilde{a}_i(t)\}$ and $\{\tilde{\tilde{a}}_i(t)\}$ must be re-expressed in terms of coefficients $\{a_i(t)\}$. The connection is given explicitly from the recurrence relation of the Chebyshev polynomial derivatives [50].

The residual is obtained by replacing the derivatives (3.4b) and (3.4c) in the diffusion equation (3.1):

$$R = \left\| \sum_{i=0}^{n} \left[\dot{a}_i(t) - \nu\,\tilde{\tilde{a}}_i(t)\right] T_i(x) \right\| \longrightarrow \min, \tag{3.5}$$

which is considered a misfit of the approximate solution. The residual is minimized via the Galerkin technique, which sets Eq. (3.5) orthogonal to the Chebyshev basis functions $\langle R, T_i \rangle = 0$. Thus, it leads to the following relation between the spectral coefficients:

$$\dot{a}_i(t) - \nu\,\tilde{\tilde{a}}_i(t) = 0, \qquad i = 0, 1, \ldots, n-2.$$

Finally, after the projection and expansion of the residual, the result is a system of Ordinary Differential Equations (ODE), with $N-2$ equations to be solved as a function of time. The

two extra coefficients are obtained by substituting the derivative (3.4a) into the boundary conditions (3.2):

$$\sum_{i=0}^{n} \tilde{a}_i(t)\,T_i(-1) \;-\; \mathrm{Bi}_{v,\mathrm{L}} \sum_{i=0}^{n} a_i(t)\,T_i(-1) \;+\; \mathrm{Bi}_{v,\mathrm{L}}\,u_{\mathrm{L}}(t) \;=\; 0\,, \tag{3.6a}$$

$$-\sum_{i=0}^{n} \tilde{a}_i(t)\,T_i(1) \;-\; \mathrm{Bi}_{v,\mathrm{R}} \sum_{i=0}^{n} a_i(t)\,T_i(1) \;+\; \mathrm{Bi}_{v,\mathrm{R}}\,u_{\mathrm{R}}(t) \;=\; 0\,, \tag{3.6b}$$

with $T_i(-1) = (-1)^i$ and $T_i(1) \equiv 1$ (see [50]). Eqs. (3.6a) and (3.6b) are written in an explicit way, with coefficients a_n and a_{n-1} expressed in terms of the other coefficients.

Therefore, the original partial differential equation (3.1) is reduced to a system of ODEs plus two algebraic expressions. For linear problems, the system of ODEs can be explicitly built. Otherwise, we have a system of Differential–Algebraic Equations. Moreover, the reduced system of ordinary differential equations has the following form:

$$\dot{a}_i(t) \;=\; \mathcal{A}\,a_i(t) \;+\; \mathrm{b}(t)\,, \qquad\qquad i \;=\; 0,\,1,\,\ldots,\,n-2\,, \tag{3.7}$$

where, $\mathcal{A} \in \mathrm{Mat}_{(n-2)\times(n-2)}(\mathbb{R})$, with constant coefficients and with $\mathcal{O}(n) \simeq 10$. Besides, $\mathrm{b}(t) \in \mathbb{R}^{(n-2)}$ is a vector coming usually from boundary conditions.

Initial values of the coefficients $\{a_i(t=0)\}$ are computed by the Galerkin projection of the initial condition [17]:

$$a_i(0) \;=\; \frac{2}{\pi\,c_i} \int_{-1}^{1} \frac{u_0(x)\,T_i(x)}{\sqrt{1-x^2}}\,\mathrm{d}x\,, \qquad\qquad i \;=\; 0,\,1,\,\ldots,\,n-2\,, \tag{3.8}$$

where, $u_0(x)$, is the dimensionless initial condition. After solving the *reduced* system of ODEs (Eqs. (3.7) and (3.8)), it is possible to compose the solution along with the Chebyshev polynomial.

Thus, by using the Spectral–ROM approach to build the reduced order model, the time-dependent coefficients $\{a_i(t)\}$ are computed by solving the following system:

$$\begin{cases} \dot{a} \;=\; \mathcal{A}\,a \;+\; \mathrm{b}(t)\,, \\ a(0) \;=\; a_0\,, \end{cases} \tag{3.9}$$

remembering that $\mathcal{A} \in \mathrm{Mat}_{s\times s}(\mathbb{R})$ is a constant coefficient matrix, $\mathrm{b}(t) \in \mathbb{R}^s$ is a vector coming from the boundary conditions and a_0 is the vector of initial spectral coefficients. The main advantage of a Spectral–ROM is that $s \ll p$, where p is the number of degrees of freedom needed to solve problem (3.2) by means of conventional methods (finite-differences, finite-elements and finite-volumes). We note that the matrix $\mathcal{A}$ and the vector $\mathrm{b}(t)$ might depend on problem parameters, such as the diffusion coefficient ν:

$$\mathcal{A} \;=\; \mathcal{A}(t;\nu)\,, \quad \text{and} \quad \mathrm{b} \;=\; \mathrm{b}(t;\nu)\,.$$

Different approaches can be used to solve the ODE System 3.9, depending on the cases considered. Interested readers are invited to consult [28] for a more profound presentation. The most straightforward way to use the Spectral–ROM from Eq. (3.9) is to apply a numerical integration scheme, *e.g.*, an adaptive Runge–Kutta with moderate accuracy,

since Eq. (3.9) is just a ROM. So, with an embedded error control and not so stringent tolerances, it can be done very efficiently.

3.2. Proper Generalised Decomposition

The Proper Generalised Decomposition (PGD) is also a model reduction method. It originates in the radial space-time separated representation proposed by Ladevèze in 1985 [38]. In 2006, the separated representations were extended to the multidimensional case by Chinesta and co-workers [6]. Interested readers may see [21, 22] for additional details on the method as well as [20] for an introduction. This strategy has been successfully applied and validated for various industrial applications. For instance, the PGD method was applied to quantum mechanics (Schrödinger equation) [5], kinetics theory (Fokker–Planck equation non-Newtonian fluids) [7, 51], phase separation in heterogeneous mixtures (Langer equation) [39], virtual surgery (forces, vibrations, *etc.*) [44], nonlinear stochastic problems (Burgers equation, 2D nonlinear diffusion problems) [45], multi-scale and multi-physics problems (visco-plasticity, damage, *etc.*) [14, 43], computational fluid dynamics (anisotherm Navier–Stokes problems) [26], and, more recently to, heat and moisture transfer in building materials [13].

The PGD solution to problem Eq. (3.1) is sought as a separated representation of functions of time t and space x:

$$u(x,t) \simeq \sum_{i=1}^{M} F^i(x)\, G^i(t). \tag{3.10}$$

The order of PGD ROM scales with $p = M \cdot (N_x + N_t)$.

3.2.1 Iterative resolution

Solving problem (3.1) numerically using the PGD method consists in calculating modes (F^i, G^i) iteratively from $i = 1$ to M. The first mode (F^1, G^1) is initialised in order to satisfy the initial and boundary conditions in all zones. At enrichment step $m < M$, we assume that a former approximation of $u(x,t)$ is known and the new couple $F^{m+1}(x) = R(x)$ and $G^{m+1}(t) = S(t)$ has to be calculated according to:

$$u(x,t) = \sum_{i=1}^{m} F^i(x)\, G^i(t) + R(x)\, S(t). \tag{3.11}$$

Eq. (3.11) is introduced into Eq. (3.1). Thanks to the separated representation of the solution $u(x,t)$ for dimensions t and x (Eq. (3.10)), we get:

$$\frac{\mathrm{d}S}{\mathrm{d}t} R - \nu S \frac{\mathrm{d}^2 R}{\mathrm{d}x} = \sum_{i=1}^{m} \frac{\mathrm{d}G^i}{\mathrm{d}t} F^i - \nu G^i \frac{\mathrm{d}^2 F^i}{\mathrm{d}x^2} + \mathrm{Res}^{m+1}, \tag{3.12}$$

where Res^{m+1} is the residual of Eq. (3.1) because Eq. (3.11) is an approximation of the solution.

3.2.2 Computing R (t) and S (x)

We are at step m searching for the new couple R and S by solving Eq. (3.12). To compute them, Eq. (3.12) will be successively projected on R and S. For this, we note the scalar product $\langle \bullet, \bullet \rangle_y$ in the domain Ω_y, defined by:

$$\langle f, g \rangle_y = \int_{\Omega_y} f\, g \, \mathrm{d}y ,$$

evaluated numerically using the discrete values of functions f and g and a trapezoidal approximation for the integral. Here, the scalar product is defined for both time and space domains.

Eq. (3.12) is projected on R, assuming $\langle \mathrm{Res}^{m+1}, R \rangle_x = 0$ to obtain:

$$\alpha_1 \frac{\mathrm{d}S}{\mathrm{d}t} - \beta_1 S = \gamma_1 , \tag{3.13}$$

with:

$$\alpha_1 = \langle R, R \rangle_x , \quad \beta_1 = \left\langle R, \nu \frac{\mathrm{d}^2 R}{\mathrm{d}x^2} \right\rangle_x , \quad \gamma_1 = \sum_{i=1}^{m} \langle R, -F^i \rangle_x \frac{\mathrm{d}G^i}{\mathrm{d}t} + \left\langle R, \nu \frac{\mathrm{d}^2 F^i}{\mathrm{d}x^2} \right\rangle_x G^i .$$

Eq. (3.12) is now projected on S, assuming $\langle \mathrm{Res}^{m+1}, S \rangle_t = 0$ and gives:

$$\alpha_2 R + \beta_2 \frac{\mathrm{d}^2 R}{\mathrm{d}x^2} = \gamma_2 , \tag{3.14}$$

with:

$$\alpha_2 = \left\langle S, \frac{\mathrm{d}S}{\mathrm{d}t} \right\rangle_t , \quad \beta_2 = \langle S, S \rangle_t , \quad \gamma_2 = \sum_{i=1}^{m} \left\langle S, -\frac{\mathrm{d}G^i}{\mathrm{d}t} \right\rangle_t F^i + \langle S, G^i \rangle_t \frac{\mathrm{d}^2 F^i}{\mathrm{d}x^2} .$$

After theses projections, to solve Eqs. (3.13) and (3.14), an alternating direction fixed-point algorithm is used. The stopping criterion, assuming the algorithm has converged, is:

$$\left\| R^q - R^{q-1} \right\| \leqslant \eta_1 \quad \text{and} \quad \left\| S^q - S^{q-1} \right\| \leqslant \eta_1 ,$$

where q is the index of iteration of the fixed-point algorithm and η_1 is a tolerance parameter chosen by the user.

3.2.3 Convergence of the global enrichment

Functions R and S have just been computed by a fixed-point algorithm. The PGD basis is enriched, noting $F^{m+1} = R$ and $G^{m+1} = S$ the new modes. The field of interest u can be written as:

$$u(x,t) = \sum_{i=1}^{m} F^i(x)\, G^i(t) + R(x)\, S(t) = \sum_{i=1}^{m+1} F^i(x)\, G^i(t) .$$

The enrichment of the PGD solution stops when the norm of the residual $\left|\left| \mathrm{Res}^{m+1} \right|\right|$ is assumed negligible with respect to η_2, another tolerance parameter chosen by the user:

$$\left\| \mathrm{Res}^{m+1} \right\| = \left\| \sum_{i=1}^{m} \frac{\mathrm{d}G^i}{\mathrm{d}t} F^i - \nu G^i \frac{\mathrm{d}^2 F^i}{\mathrm{d}x^2} \right\| \leqslant \eta_2 .$$

3.3. Comparison of the numerical solution

To compare and validate the proposed methods, the error between the solution $u(x,t)$, obtained by one of numerical the methods, and the reference solution u^{ref}, is computed as a function of x by the following formulation:

$$\varepsilon_2(x) \overset{\mathrm{def}}{:=} \sqrt{\frac{1}{N_t} \sum_{j=1}^{N_t} \left(u_j^{\mathrm{num}}(x,t) - u_j^{\mathrm{ref}}(x,t) \right)^2},$$

where N_t is the number of temporal steps. The global uniform error ε_∞ is given by the maximum value of $\varepsilon_2(x)$:

$$\varepsilon_\infty \overset{\mathrm{def}}{:=} \sup_{x \in [0,L]} \varepsilon_2(x) .$$

The computation of the reference solution $u^{\mathrm{ref}}(x,t)$ is detailed in further Sections.

4. Linear transfer in porous material

The first case of linear moisture transfer is considered from [11, 53] to analyze the moisture buffer effects in a 500-mm aerated concrete under isothermal condition, at a temperature of 23 °C. The vapor permeability is $d_m = 3 \cdot 10^{-11}$ s and its moisture storage is $c_m = 1.85 \cdot 10^{-4}$ kg/m^3/Pa [11]. The uniform initial vapor pressure in the material is $P_v^i = 842$ Pa, corresponding to a relative humidity of 30 %. The total time of simulation corresponds to 120 h. The left boundary is set to a constant vapor pressure, identical to the initial condition. At the right boundary, the relative humidity varies sinusoidally between 33 % and 75 %, with a period of 24 h. The convective vapor transfer coefficient is set to $2 \cdot 10^{-8}$ s/m.

The solution of the problem has been computed for a discretization of $\Delta x^\star = 5 \cdot 10^{-3}$ and $\Delta t^\star = 10^{-1}$. The physical phenomena are well represented, as illustrated in Figure 1(a) with the time evolution of the relative humidity at $x = 0.47$ m. The variations follow the ones of the right boundary conditions and, the diffusion process goes towards the periodic regime. It can be noted a good agreement between the two reduced order models. Furthermore, the vapor pressure profile is shown in Figure 1(b) for $t = \{20, 80, 120\}$ h, enhancing the good accuracy of the solution to represent the physical phenomenon.

The absolute error of the reduced order model is of the order of $\mathcal{O}\left(10^{-4}\right)$, as illustrated in Figure 2(a). The methods are compared with a reference solution, which has been computed using the `Matlab` open source toolbox `Chebfun` [25]. To give a solution with this order of accuracy, the PGD needed 22 modes, while the Spectral only required 9 modes. It corresponds to 21 and 7 degrees of freedom, respectively. Figure 2(b) presents the error ε_∞ as a function of the number of modes. As we increase the number of modes, the solution of the Spectral–ROM converges faster than the PGD solution because the convergence of the Spectral method is exponential. To illustrate the convergence of the solution, the profile of the vapor pressure for the last time instant of simulation is represented with different numbers of modes in Figures 3(a) and 3(b) for the PGD and the Spectral–ROM, respectively.

The reduced system of ODEs, of size 7 is implemented in `Matlab`, and the spectral coefficients $\{a_n(t)\}$ are computed for any intermediate time instants by the solver `ODE45` [55]. These spectral coefficients are shown in Figure 4(a). It can be seen that the first coefficients have the highest magnitude making the solution to converge with a few modes (an order of 10), which happens thanks to the fact that the Chebyshev polynomials have excellent approximation properties for smooth function. In addition, the last coefficient determines the magnitude of the residual, implying that the error will not be lower than the magnitude of the last coefficient a_n, as explained in [28]. A brief comparison with an analytical solution, built on Fourier decomposition [47], reveals that the eigenvalues of the Spectral method decrease faster, as shown in Figure 4(b). Note that eigenvalues of the analytical solution do not have to coincide with the ones of the Spectral method since the basis functions are not the same for the Chebyshev polynomials and the trigonometric ones.

Regarding the PGD, Figures 5(a) and 5(b) present the first modes, depending on time and space, respectively. They do not have a physical meaning and constitute a separated representation of the solution. Their tensorial product enables to compute the solution of the problem. It is a similar approach for the Spectral–ROM, where the coefficients $a_n(t)$ are multiplied by the Chebyshev polynomials.

Remarks on *a posteriori* POD method

Here, the purpose is to compare the PGD and Spectral model order reduction to the well-established POD approach. For this, the reference solution u obtained with the `Chebfun` package was used to compute the correlation matrix R, with elements $\{r_{ik}\}$ given by:

$$r_{ik} = \sum_{j=1}^{N_t} u(x_i, t_j)\, u(x_k, t_j).$$

Then, the singular values λ of the correlation matrix are computed. A truncation is operated in the eigenvectors basis to define ϕ_i the spatial basis function composed of the Q eigenvectors of the correlation matrix r. Thus, the solution of the POD reduced

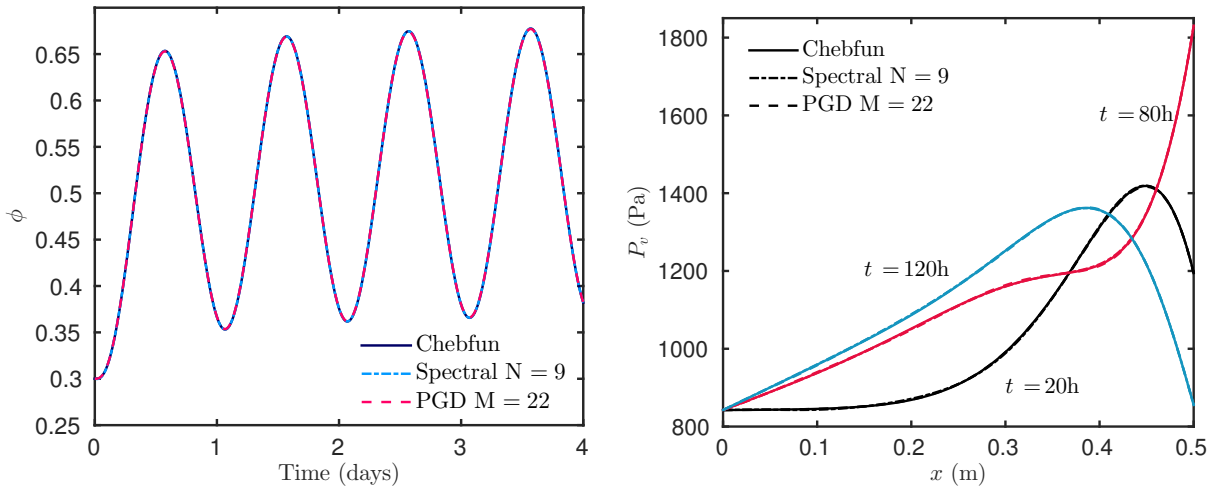

Figure 1. *(a) Relative humidity at the right boundary as function of time, and (b) pressure vapor profiles for* $t = \{20\,,80\,,120\}$ h .

order model (POD–ROM) approximates the solution of the problem by:

$$u\,(x\,,t\,) \;\approx\; u_Q\,(x\,,t\,) \;\overset{\text{def}}{:=}\; \sum_{i=0}^{Q} a_i\,(t\,)\,\phi_i\,(x\,)\,,$$

where Q is the number of modes corresponding to the model order reduction. For this case study, Figure 6(a) shows the convergence of the solution obtained with a POD reduced order model. Moreover, Figure 6(b) presents the error with the reference solution as a function of the modes Q . The solution of the POD–ROM converges faster than the PGD and Spectral approaches. Only $Q \;=\; 5$ modes are sufficient to compute a solution accurate to the order $\mathcal{O}\,(10^{-3})$, which is lower than the one for the PGD or Spectral–ROM for the same accuracy. However, as underlined in the Introduction section, the POD approach is *a posteriori*. To build the POD reduced order model, a preliminary computation of the solution was required, which is a non-negligible restriction.

5. Computing parametric solution using reduced order models

Challenging problems appear from practical applications of building performance assessment. Consider, for instance, the analysis of the wall behavior in terms of heat and mass transfer, as a function of different parameters such as thermal inertia, vapor permeability, insulation thickness, among others. In the context of environmental issues and thermal regulations, the wall behavior may be optimized as a function of those parameters. Several studies of parametric simulations are presented in the literature. In [3, 4, 9, 15, 34, 46, 59],

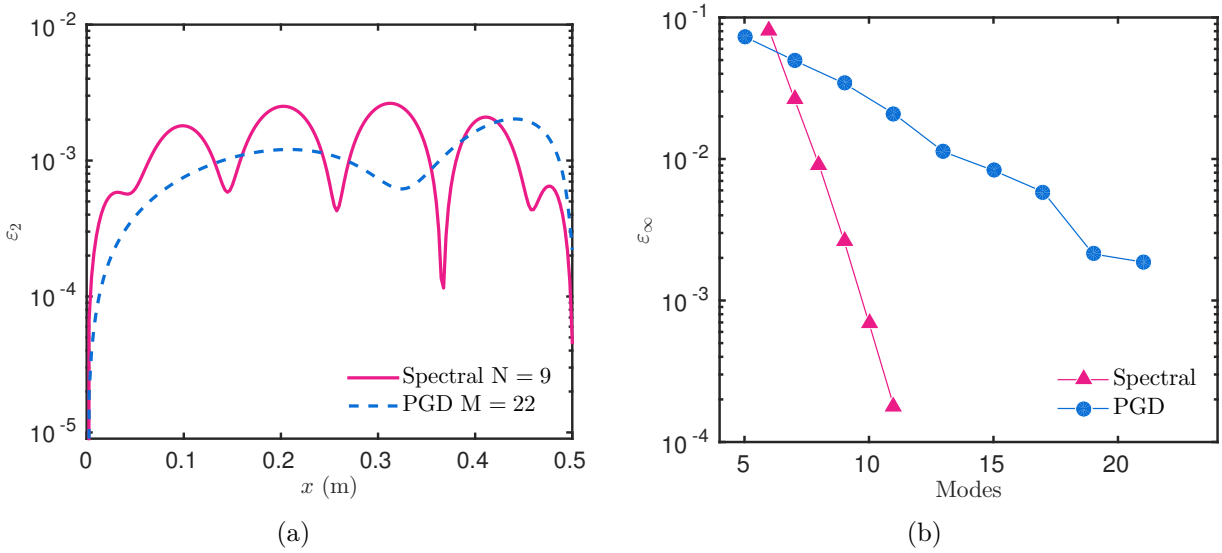

Figure 2. *(a) Error as a function of x (m) and (b) error as a function of the number of modes.*

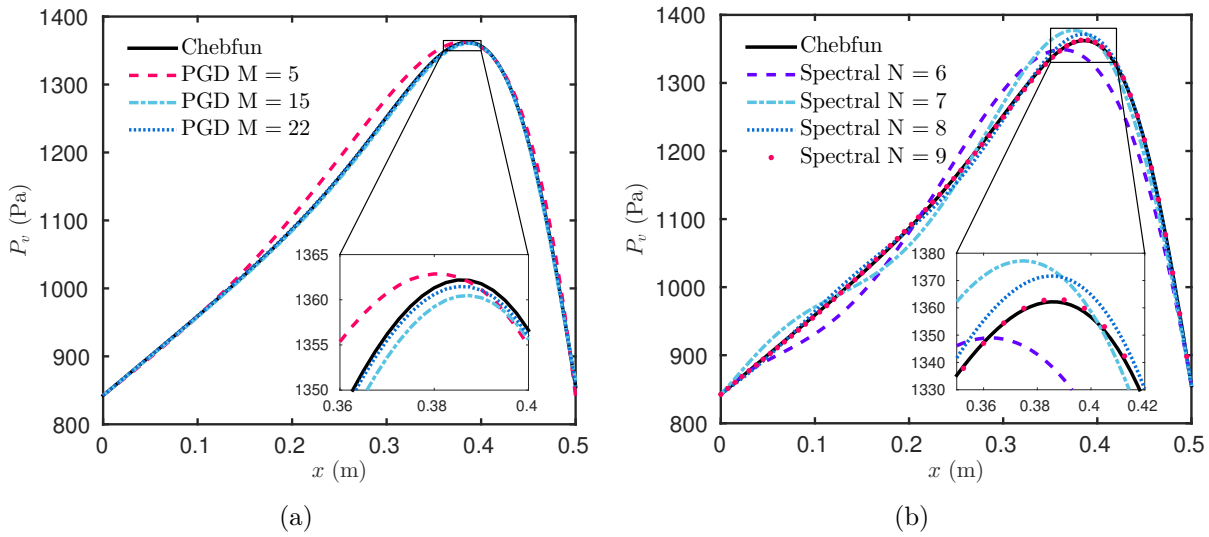

Figure 3. *Vapor pressure profiles for different number of modes (a) for the PGD and (b) for the Spectral–ROM.*

numerical methods are used to determine the optimum insulation thickness of different wall configurations. In [8], the influence of wall thermal inertia on the energy consumption was investigated by using the `EnergyPlus` program for 24 construction types. In [37], the MBV of five hemp concrete materials were assessed using a numerical method. Those parametric simulations are based on models using numerical methods due to almost no restriction in terms of boundary conditions, geometry, material properties, among other considerations.

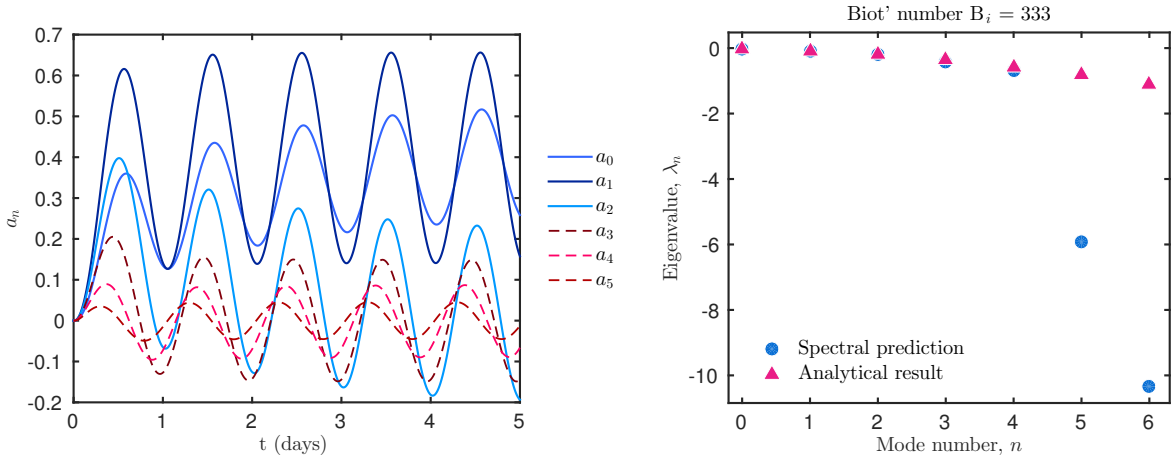

Figure 4. *(a) Spectral coefficients as sets of time and, (b) Eigenvalues of the Analytical and of the Spectral solution corresponding to the first modes.*

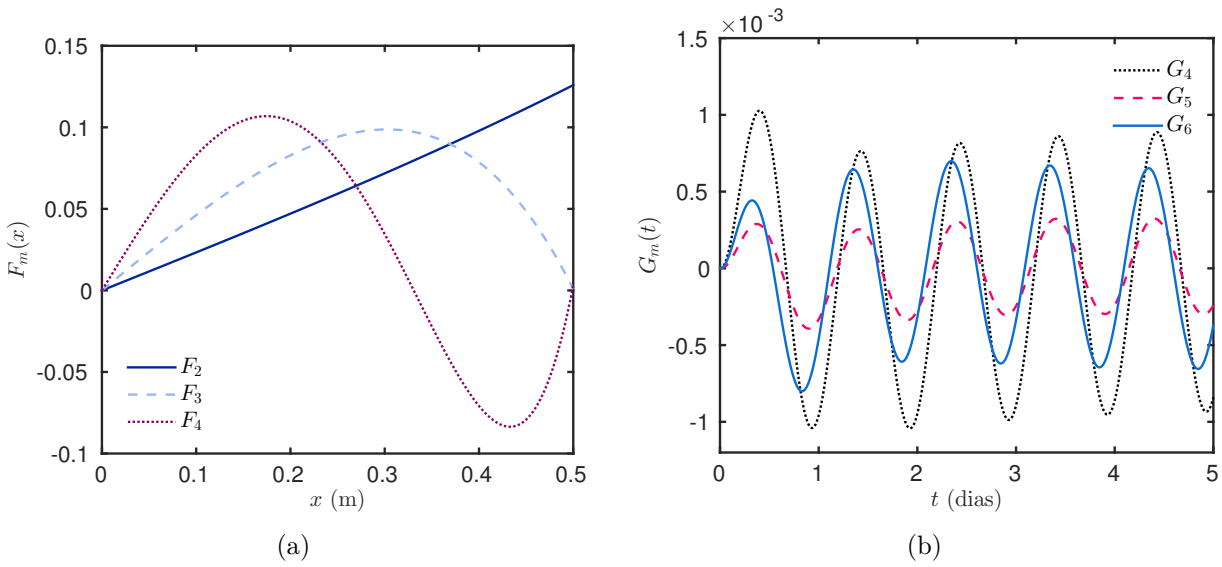

Figure 5. *(a) F_m tensor function; (b) G_m tensor function.*

Nevertheless, for parametric studies, they require large numbers of simulations. Indeed, the numerical model is not dependent on the parameters of interest. Thus, a computation of the numerical model is required for each value of the parameters within their domain of variation, demanding a high calculation cost, even after the dramatic evolution of computer hardware since the 1970's. Therefore, reduced order model can be used to perform efficient parametric studies with a limited computational costs.

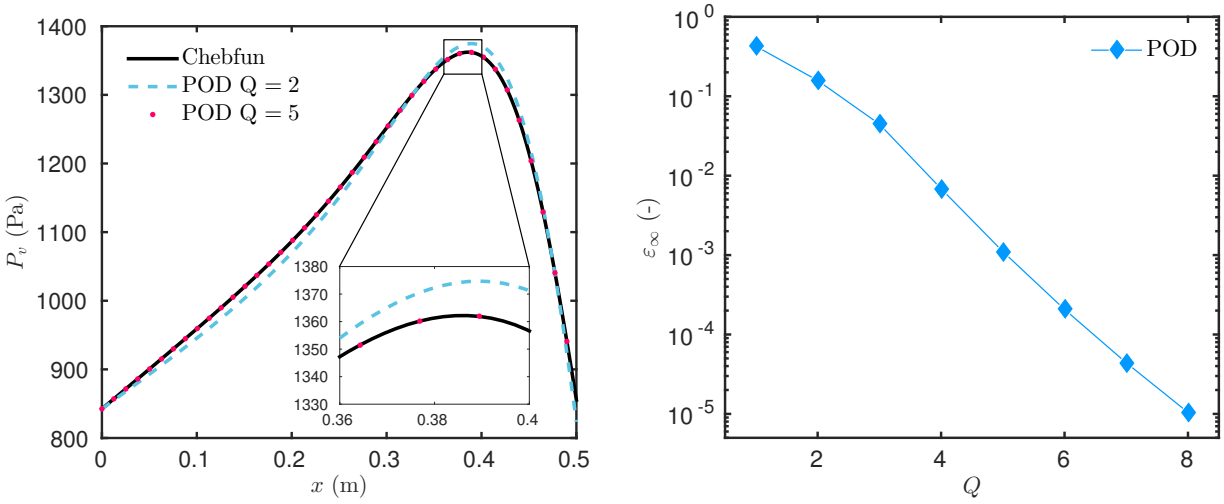

(a) (b)

Figure 6. *Vapor pressure profiles for different number of modes computed with the POD (a) and the error ε_∞ as a function of the number of modes Q (b).*

5.1. Extension of model reduction techniques to parametric problems

The issue of solving a parametric problem is to compute the solution u of Eq. (3.1) depending on the usual time and space coordinates x and t as well as the parameter ν of the problem. Thus, the solution is seek as $u(x,t;\nu)$, where ν is defined as a coordinate of the problem within a given interval $\nu \in [\nu_{\min}, \nu_{\max}]$. Here we note N_ν the number of elements (cardinal) of the domain $[\nu_{\min}, \nu_{\max}]$.

5.1.1 Spectral reduced order model

For the parametric study, we want to compute the solution as a function of $(x,t;\nu)$:

$$u(x,t;\nu) \approx u_n(x,t;\nu) = \sum_{n=0}^{N} a_n(t;\nu)\,\phi_n(x).$$

The basis function will always depend only on x, that is why the parameter ν is computed with spectral coefficients $\{a_n(t;\nu)\}$. As it is not straightforward to compute the coefficients $a_n(t;\nu)$ depending on both parameters, we compute the solution for each value of the parameter ν, using a loop. The latter can easily be parallelised on high-performance computer systems. It would be possible to vectorize the computation of the parametric Spectral–ROM solution although the method would significantly loose its speed calculation.

5.1.2 PGD reduced order model

To compute a parametric solution of Eq. (3.1) $u(x,t;\nu)$, the PGD approach assumes a separated tensorial representation of the solution:

$$u(x,t;\nu) \approx u_m(x,t;\nu) = \sum_{m=1}^{M} F^m(x)\, G^m(t)\, H^m(\nu).$$

Functions $\left(F, G, H\right)$ are computed following the methodology described in Section 3.2. Interested readers may refer to [12, 19, 21] for complementary details on the methodology. The important point, is that the solution u is computed *at once* as a function of the coordinates x, t and ν.

5.2. Case study

For this case, we seek for a parametric solution of problem Eq. (2.4). The vapor pressure is computed as a function of time t, space x and moisture storage capacity c_m. As in the previous case, simulations are preformed in order to reproduce experiments that estimate the moisture buffer value of the materials. Thus, the right boundary condition is exposed to cyclic changes of relative humidity between 33 % and 75 %, with a 24 h period. The total time of simulation is still 120 h. The convective vapor coefficient is $h_v = 2 \cdot 10^{-8}$ s/m. The left boundary is set to a constant vapor pressure, identical to the initial condition $P_v^i = 842$ Pa. Simulations undergo at a constant 23 °C temperature. All 500-mm materials have the same vapor permeability, $d_m = 2.4 \cdot 10^{-11}$ s, while the moisture storage capacity varies in the interval $\Omega_c = 1.2 \cdot 10^{-3}$ and $6 \cdot 10^{-3}$ kg/m³/Pa [53].

First, we perform a simulation for 10 different values of moisture storage capacity in the interval Ω_c, representing different kinds of materials. Two different techniques of reduction order models were employed, the PGD and the Spectral–ROM. To validate these methods, results were compared to the reference solution, constructed with the `Chebfun` package for `Matlab`.

Figure 7(a) shows the mass content of each material among the simulation time. Even with a low difference between the highest and the lowest values of storage capacity, it is possible to observe significant variations of the weight as the the storage capacity increases, retaining more moisture. Furthermore, Figure 7(b) presents the weight for the two highest values of moisture storage capacity, corresponding to $6{\cdot}10^{-3}$ and $4.15{\cdot}10^{-3}$ kg/m³/Pa. The last profile of the pressure vapor for all values of moisture storage capacity is represented in Figure 8(a). In these figures, the PGD and the Spectral–ROM are in a good agreement with the reference solution.

To compute the parametric study, with the same order of accuracy, the PGD needed around $M = 100$ modes, while the Spectral–ROM used only $N = 11$ modes. This difference comes from the nature of the methods, that are constructed by different ways. The error ε_∞ is shown as a function of the storage capacity values in Figure 8(b). The methods were constructed in order to give the same order of accuracy, around $\mathcal{O}(10^{-3})$. It should

be noted that the Spectral–ROM can give more accurate results, with the same degrees of freedom, by increasing the tolerance in the `ODE45` `Matlab` function, when the reduced system is being computed. The degrees of freedom of the Spectral–ROM were predetermined based on the previous case and by the order of the parameters values. Meanwhile, the PGD computes its solution if the residual is lower than a given tolerance. The rate of convergence of the PGD approach is illustrated in Figure 9, presenting the error as a function of the number of modes.

The numbers of operation for each approach can be estimated, remembering N_x and N_t stand for the number of elements according to the discretization of the space and time domains, respectively. The quantity N_ν represents the number of elements of parameter c_m considered for the parametric study. A standard approach based on implicit Euler schemes requires $N_x \cdot N_t \cdot N_\nu$ operations. Considering the discretization parameters to reach the given accuracy $N_t = 1.2 \cdot 10^5$ and $N_x = 4 \cdot 10^2$, the number of operations scales with [29]:

$$\text{Euler implicit:} \qquad \mathcal{O}\left(N_x \cdot N_t \cdot N_\nu\right) \simeq \mathcal{O}\left(4.8 \cdot 10^7 \cdot N_\nu\right).$$

For the Spectral–ROM, the number is related to the solution of the ODE system Eq. (3.7), computed in this case with the `Matlab` `ODE45` solver. It is based on the iterative Runge–Kutta method to approximate the solution. The number of operation depends on the tolerance of the solver, which has a maximum tolerance of $\sim 10^{-5}$ for `ODE45`. Thus, we have:

$$N_t \simeq \frac{T}{\Delta T} \simeq \frac{T}{(\mathsf{tol})^{1/5}},$$

where T is the total time of simulation. At each time step, the Runge–Kutta needs to compute six times the vector product $\mathcal{A}_{n\times n}$, where n depends on the degree of freedom N of the solution ($n = N - 2$). Thus, it leads to $6 \cdot n^2$ operations to perform, knowing that n scales with 10. Consequently, the total number of operations for the Spectral–ROM scales with:

$$\mathcal{O}\left(\frac{6\,(N-2)^2\,T}{(\mathsf{tol})^{1/5}}\right).$$

For this parametric case, knowing that the tolerance was set to 10^{-3}, with $N \simeq 11$ modes, the number of operations performed by the Spectral–ROM is expressed as:

$$\text{Spectral–ROM:} \quad \mathcal{O}\left(\frac{6\,(11-2)^2\,T}{(10^{-3})^{1/5}}\,N_\nu\right) \simeq \mathcal{O}\left(2.3 \cdot 10^5 \cdot N_\nu\right).$$

Therefore, the number of operations increases faster for the Spectral–ROM and for the standard Euler methods than for the PGD approach. After some kind of initial investment, the increase in the number of operations for the PGD is much slower than for other approaches. The advantage of the PGD, in this case, it is related to its ability to compute *at once* the solution depending on the three coordinates, whereas the Spectral–ROM computes the solution for each value of moisture storage capacity independently, by a loop. It should be noted that the Euler approach, based for instance on backward time centered

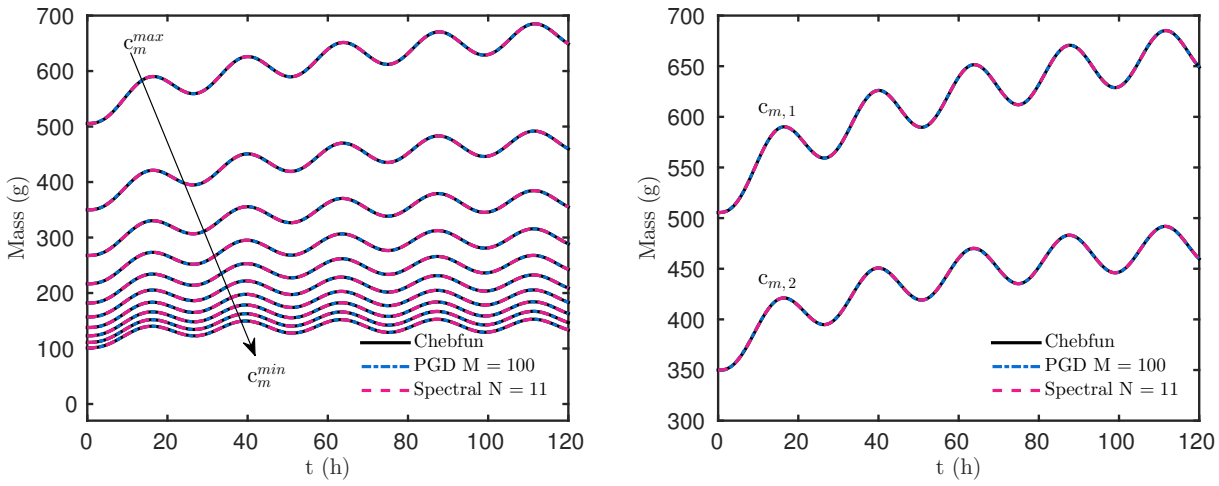

(a) (b)

Figure 7. *(a) Water content increase for all values of parameter c_m, and (b) Water content increase for the two highest values of moisture storage capacity.*

space, is a low order approximation of the solution, providing a less accurate solution than the Spectral–ROM. An interesting advantage of the PGD is the low storage cost of the solution thanks to the tensorial representation of the solution. This feature may be particularly interesting for real time applications. These features also impact the CPU time of each algorithm, which has been evaluated using `Matlab` platform on a computer with Intel i7 CPU and 8GB of RAM. Figure 10 shows the CPU time as a function of the number of elements of the parameter c_m. For comparison, the CPU time required using the EULER implicit scheme is also reported. Since the Spectral–ROM has a reduced system to solve, its computational time drops significantly when compared to traditional methods. However, the loop to simulate the parametric study increases the CPU time linearly with the number of elements. For few numbers of elements of parameter c_m, around 20, the Spectral–ROM is faster than the PGD. Yet, if the number of elements increases, the PGD is a more attractive method. In addition, the large original model, based on implicit EULER scheme, requires an important extra CPU time to compute the parametric solution.

6. Nonlinear transfer in porous material

The last case considers nonlinear transfer with moisture-dependent material properties. Therefore, the diffusion coefficient ν depends on the field u and Eq. (3.1) becomes:

$$\frac{\partial u}{\partial t} = \boldsymbol{\nabla} \cdot \Big(\nu(u) \boldsymbol{\nabla} u \Big). \tag{6.1}$$

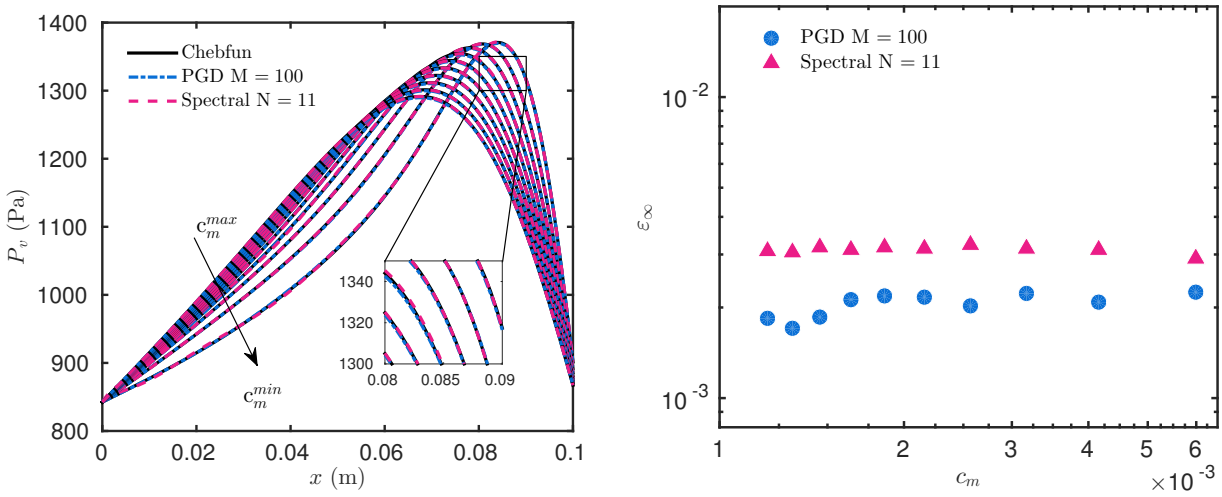

(a) (b)

Figure 8. *(a) vapor pressure profiles at* $t = 120\,\mathsf{h}$ *, for* $c_m \in [1.2 \cdot 10^{-3}; 6 \cdot 10^{-3}]$ $\mathsf{kg/m^3/Pa}$ *, and (b) the error in function of all values of moisture storage capacity between this interval.*

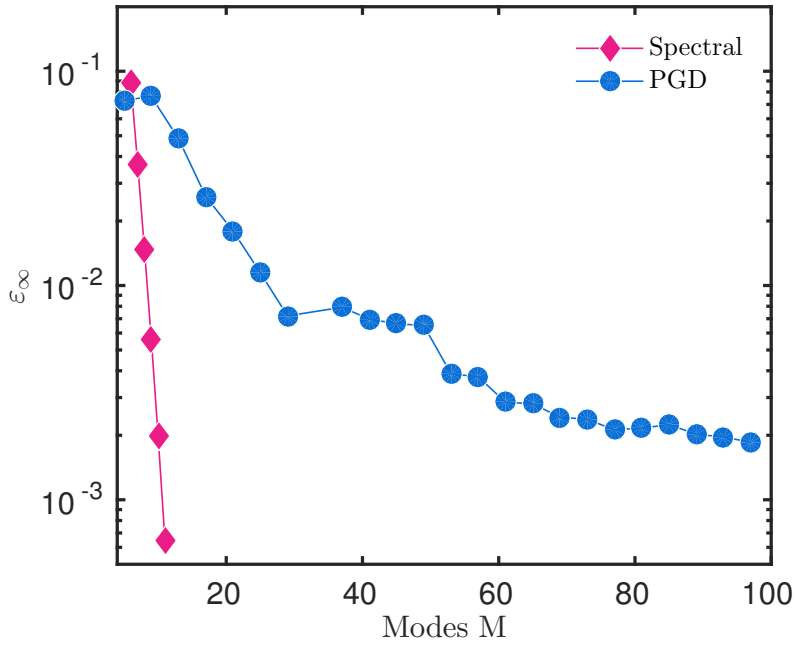

Figure 9. *Error computed for* $c_m = 1.46 \cdot 10^{-3}\,\mathsf{kg/m^3/Pa}$ *in function of the number of modes* M *.*

6.1. Extension of model reduction techniques to nonlinear problems

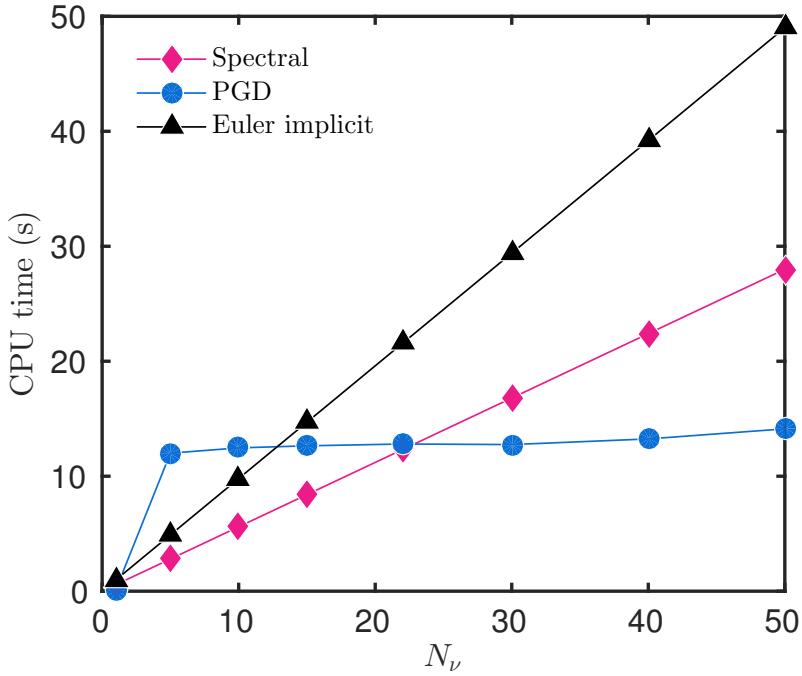

Figure 10. *CPU time* (s) *as a function of the number of elements* N_ν *of parameter* c_m.

6.1.1 Spectral reduced order model

In order to apply better the Spectral method, Eq. (6.1) is rearranged as follows:

$$\frac{\partial u}{\partial t} = \nu(u)\frac{\partial^2 u}{\partial x^2} + \lambda(u)\frac{\partial u}{\partial x}, \tag{6.2}$$

where,

$$\nu(u) \stackrel{\text{def}}{:=} \frac{d_m(u)}{c_m(u)},$$

$$\lambda(u) \stackrel{\text{def}}{:=} \frac{1}{c_m(u)} \cdot \frac{\mathrm{d}\Big(d_m(u)\Big)}{\mathrm{d}u}.$$

By using Spectral methods the unknown $u(x,t)$ is approximated by the finite sum (3.3) and, the derivatives can be written so that the Chebyshev polynomials remain the same, as in the linear case of Eq. (3.4). Thus, Eq. (6.2) becomes:

$$\sum_{i=0}^{n} \dot{a}_i(t)T_i(x) = \nu\left(\sum_{i=0}^{n} a_i(t)T_i(x)\right)\sum_{i=0}^{n}\tilde{\tilde{a}}_i(t)T_i(x) + \lambda\left(\sum_{i=0}^{n} a_i(t)T_i(x)\right)\sum_{i=0}^{n}\tilde{a}_i(t)T_i(x). \tag{6.3}$$

The nonlinear terms $\nu\left(\sum_{i=0}^{n} a_i(t)\,T_i(x)\right)$ and $\lambda\left(\sum_{i=0}^{n} a_i(t)\,T_i(x)\right)$ are treated by applying the Galerkin projection and the Chebyshev–Gauß quadrature [28]. Contrary to the linear case, the boundary conditions cannot provide an explicit expression for the two last coefficients $a_n(t)$ and $a_{n-1}(t)$. Thus, it is not possible to compute the solution in the same way. Although, with all elements listed before, it is possible to set the system to be solved by composing an ODE system with two additional algebraic expressions for the boundary conditions. It results in a system of Differential–Algebraic Equations (DAEs) with the following form:

$$\mathcal{M}\,\dot{a}_n(t) \;=\; \mathcal{A}\,a_n(t) \;+\; \mathrm{b}(t),$$

where, $\mathcal{M}$ is a diagonal and singular matrix ($\mathrm{rank}(\mathcal{M}) = n-2$) containing the coefficients of the Chebyshev weighted orthogonal system, $\mathrm{b}(t)$ is a vector containing the boundary conditions and, $\mathcal{A}\cdot a_n(t)$ is composed by the right member of Eq. (6.3). The initial condition is given by Eq. (3.8) and the DAE system is solved by `ODE15s` or `ODE23t` from `Matlab`. As for the linear case, interested readers may consult [28] for further details.

6.1.2 PGD reduced order model

To treat the nonlinearity of the problem, at the enrichment step $m < M$, the nonlinear term $\nu(u)$ is approximated using the solution from previous steps:

$$\nu(u) \;=\; \nu\left(\sum_{i=1}^{M} F^i(x)\,G^i(t) \;+\; R(x)\,S(t)\right) \;\simeq\; \nu\left(\sum_{i=1}^{M} F^i(x)\,G^i(t)\right).$$

Then, the matrix of the coefficient ν is separated into a tensorial product in the space and time directions, using a *Singular Value Decomposition* (SVD) [33] or a *Discrete Empirical Interpolation Method* (DEIM) [2, 18]:

$$\nu(u) \;=\; \sum_{j=1}^{K} \nu_t^j(x)\,\nu_x^j(t).$$

This decomposition enables us to separate the coefficient into a component depending on the coordinate of the problem. Therefore, Eq. (3.12) becomes:

$$\frac{\mathrm{d}S}{\mathrm{d}t}\,R \;-\; \sum_{j=1}^{K} \nu_t^j\,S\,\nu_x^j\,\frac{\mathrm{d}^2R}{\mathrm{d}x} \;=\; \sum_{i=1}^{m} \frac{\mathrm{d}G^i}{\mathrm{d}t}\,F^i \;-\; \sum_{j=1}^{K} \nu_t^j\,G^i\,\nu_x^j\,\frac{\mathrm{d}^2F^i}{\mathrm{d}x^2} \;+\; \mathrm{Res}^{m+1}.$$

Functions R and S are then computed using a similar approach as the one described in Section 3.2.

6.2. Case study

The material investigated is the wood fiber, which properties have been presented in [52]. The moisture transport coefficient d_m is assumed as a first-degree polynomial of the

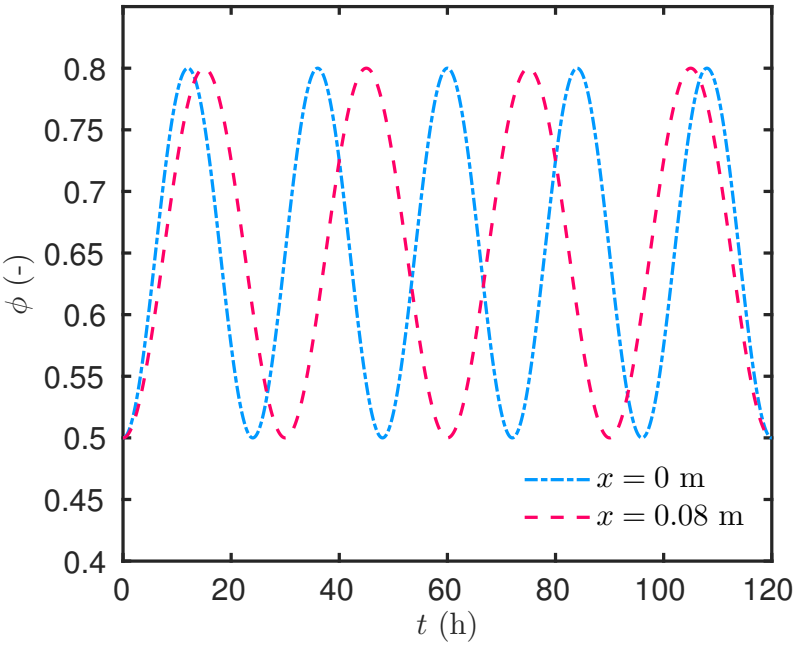

Figure 11. *Time evolution of the boundary condition.*

relative humidity, while the moisture capacity c_m as a second-degree polynomial:

$$c_m(\phi) = 120\,\phi^2 - 98\,\phi + 27.02\,, \qquad \mathsf{kg/m^3/Pa}\,,$$
$$d_m(\phi) = \left(5.65\,\phi + 2.33\right)\cdot 10^{-11}\,, \qquad \mathsf{s}\,.$$

In terms of boundary conditions, a ROBYN-type is assumed for both sides of the material, as described in Eq. (2.3). The variation of the relative humidity of the ambient air is given in Figure 11. Variations were chosen in order to excite the material in the hygroscopic region of the properties. The vapor convective transfer coefficients are set to $h_{v,\mathrm{L}} = 1\cdot 10^{-8}\mathsf{s/m}$ and $h_{v,\mathrm{R}} = 1.5\cdot 10^{-8}\,\mathsf{s/m}$. As for the previous case, the time simulation is fixed to 5 days.

Results have been computed using discretization parameters $\Delta x^\star = 10^{-2}$ and $\Delta t^\star = 10^{-2}$ for both methods. The Spectral–ROM has been built for $N = 8$ modes while the PGD for $M = 30$ modes. both results have been compared to a reference solution computed with the open source package `Chebfun`. Profiles of relative humidity in the material are shown in Figure 12(a). The time evolution of relative humidity at $x = 0.074\,\mathsf{m}$ is given in Figure 12(b). A very good agreement is highlighted between the solutions. The physical phenomena are accurately represented. The relative humidity at $x = 0.074\,\mathsf{m}$ increases according to the variation of the boundary conditions. The reduced order models have been built to give the same order of accuracy $\mathcal{O}(10^{-3})$ as illustrated in Figure 13(a). It can be noted that the PGD needs $M = 30$ modes to compute the solution of the nonlinear problem, while only $M = 22$ modes were required in the linear case. The Spectral–ROM only needs one extra mode compared to the linear case. The error with the reference solution is given as a function of the number of modes for both reduced order models in

Figure 13(b). Again, the Spectral–ROM converges faster to an accurate solution than the PGD approach. A limit is observed in the error of the Spectral–ROM, around $\mathcal{O}(10^{-4})$, due to the tolerance of the `Matlab` solver that was set to this value.

The CPU time of each method has been evaluated for the same order of accuracy of the solution and are reported in Table 1. For the comparison, the CPU time required with the classical Euler implicit scheme is also indicated. Both methods enable significant computational savings, 95 % and 99.1 % for the PGD and Spectral, respectively. The PGD requires more time than the Spectral–ROM, mainly due to the treatment of the nonlinearity of the problem. It can be noted that using the DEIM for the treatment of the nonlinearity permits to reduced by more than two the CPU time of the PGD, compared to the SVD. Indeed, in the latter case, at each iteration, the solution has to be composed to evaluate the nonlinear coefficients and then separate them along each coordinate of the problem. The CPU time of each approach is related to the number of operations. For the PGD, it scales with:

$$\text{PGD:} \qquad \mathcal{O}\left(M \cdot \left(S \cdot \left(N_t + N_x\right) + N_{\text{nl}}\right)\right),$$

where N_{nl} represents the number of operations for the treatment of nonlinearities. Depending on the method used for the decomposition of the solution, the number of operations scales with:

$$\text{SVD:} \qquad N_{\text{nl}} \approx \mathcal{O}\left(N_x^2 \cdot N_t\right),$$

$$\text{DEIM:} \qquad N_{\text{nl}} \approx \mathcal{O}\left(K \cdot \left(N_x + N_t\right)\right),$$

where $K \approx \mathcal{O}(3)$ is the order of the decomposition of the coefficients. It can be understood why the CPU time of the PGD using the DEIM is lower.

For the Spectral–ROM, thanks to the analytical pre-treatment of the solution, there is almost no increase in the number of operations. According to Eq. (6.2), the number of operations is only multiplied by two:

$$\text{Spectral–ROM:} \qquad \mathcal{O}\left(2\,\frac{6\,(N-2)^2\,T}{(10^{-3})^{1/5}}\right).$$

For the large original model, using the Euler implicit scheme, the number of operations equals [29]:

$$\text{Euler implicit LOM:} \qquad \mathcal{O}\left(N_{\text{nl}} \cdot N_x \cdot N_t\right).$$

For this case, the average number of sub-iterations required required for the implicit scheme to treat the nonlinearity was around $N_{\text{nl}} \sim \mathcal{O}(12)$ for a tolerance fixed to $0.01 \cdot \Delta t^\star$.

7. Conclusion

Due to moisture-dependent material properties and weather driven boundary conditions, numerical methods are used to compute the solution of moisture transfer problems. Usual

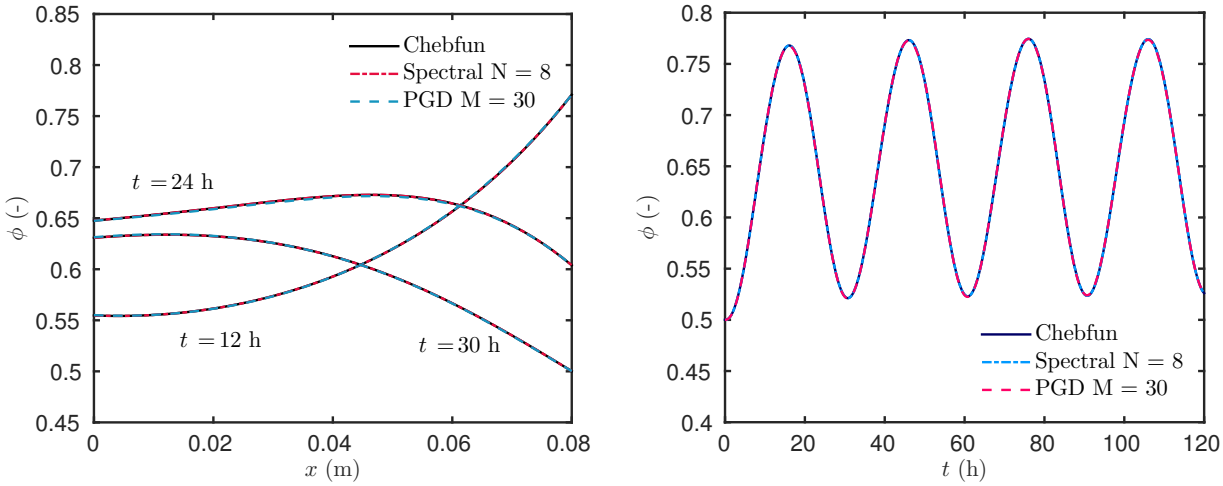

Figure 12. *(a) Relative humidity profiles in the material and (b) relative humidity evolution at* $x = 0.074\,\mathsf{m}$.

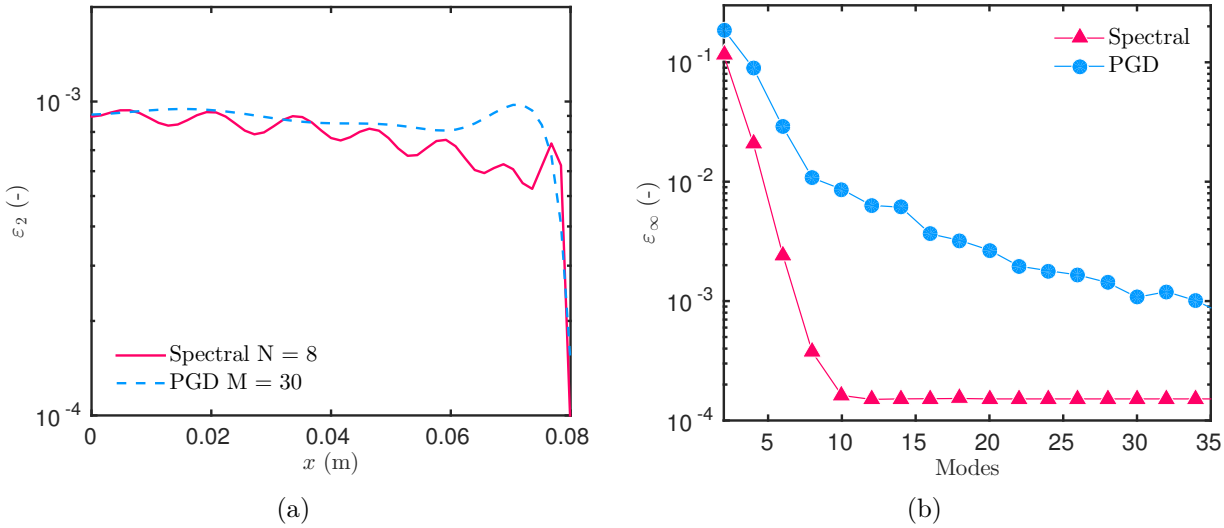

Figure 13. *(a) Error as a function of* $x\,(\mathsf{m})$ *and (b) error as a function of the number of modes.*

approaches based for instance on Euler or Crank–Nicolson schemes require the solution of large systems of equations, which imposes important numerical costs. Model reduction techniques appear then as efficient alternatives, enabling to reduce the model order without deteriorating the representation of the physical phenomena. These methods aim at preserving the computation resources in terms of CPU time and memory. Among the *a priori* model reduction techniques applied in building physics, this paper intended to compare the Spectral and the PGD methods.

Table 1. *Computational cost of the methods for the nonlinear case.*

Method	CPU time (s)	CPU time (%)
Euler implicit	36	100
PGD using SVD	5.29	15
PGD using DEIM	1.9	5
Spectral–ROM	0.35	0.9

The two reduced order methods assume that the solution is approximated by a finite sum of functions products. The Spectral method fixes a set of basis function for the space domain. Here the Chebyshev polynomials have been chosen. Analytical preliminary treatment of the Spectral solution has been operated to set an ordinary system of equations to compute the temporal coefficients of the solution. On the other hand, the PGD has no assumptions and attempt to compute directly the basis functions by minimizing the equation residual. The comparison was carried out for three cases, commonly found in building physics. The first one deals with linear moisture transfer. The second one aimed at computing a parametric solution, whose model outputs depend not only on the space and time coordinates, but also on the moisture capacity of the material. The last case dealt with a nonlinear transfer problem, with moisture dependent material properties.

Results have demonstrated that both reduced order models, Spectral and PGD, accurately represent the moisture transfer and both approaches provide an important reduction of the model order. While the order of the large original model scales with several hundred, the one of the ROMs is proportional to a few tens or even less. For the nonlinear case, thanks to this order reduction, the model reduction techniques enable to save more than 95 % of the CPU time, compared to a large original model based on a Euler implicit scheme. If both methods are efficient, some distinctions between the two ROMs have been highlighted. For the linear and nonlinear cases, the Spectral–ROM has a lower order than the PGD, $N \simeq \mathcal{O}(8)$ against $M \simeq \mathcal{O}(20)$ to $\simeq \mathcal{O}(30)$, for the same accuracy. Moreover, the error of the Spectral–ROM decreases faster with the number of modes than the PGD. For these reasons, the Spectral–ROM is faster than the PGD. For the nonlinear case, the CPU time of the Spectral–ROM is divided by 5 compared to the PGD. For the parametric case study, the two approaches compute the solution by different processes. The Spectral–ROM computes a solution for each numerical value of the material properties within a defined interval. Then, a loop is operated to compute the solution for each value of the material properties. The PGD approach considers directly the material properties as a coordinate of the problem within a defined interval of values. The solution is approximated by a tensorial representation and a basis of functions of each of the three coordinates is computed. Thus, the parametric solution is obtained *at once*. If the PGD ROM needs more modes than the Spectral method, the number of operations to compute the solution is smaller. Moreover, the increase of operations for the PGD is much slower, in this case,

thanks to the tensorial representation of the solution. For a parametric solution depending on 50 values of material properties, the CPU time of the PGD is six times faster.

To conclude the comparison of the two model reduction techniques, results have highlighted that the Spectral approach is more efficient in terms of order reduction, preserving computational resources for linear and nonlinear moisture diffusion problems. For the computation of parametric solutions, the PGD appears to be more efficient. These promising results encourage further investigation for two- or three-dimensional problems including combined heat and moisture transfer phenomena, where the order of the large original model becomes even higher.

Acknowledgments

The authors acknowledge the Brazilian Agencies CAPES of the Ministry of Education and CNPQ of the Ministry of Science, Technology and Innovation, for the financial support.

A. Nomenclature

	Latin letters	
c_m	moisture storage capacity	[kg/m^3/Pa]
d_m	moisture diffusion	[s]
g	liquid flux	[kg/m^2/s]
h_v	vapour convective transfer coefficient	[s/m]
k	permeability	[s]
L	length	[m]
P_c	capillary pressure	[Pa]
P_s	saturation pressure	[Pa]
P_v	vapour pressure	[Pa]
R_v	water gas constant	[J/kg/K]
T	temperature	[K]
	Greek letters	
ϕ	relative humidity	[−]
ρ	specific mass	[kg/m^3]

B. Dimensionless values

B.1. Linear case

Problem (2.4) is taken into account with $g^\star_{l,\mathrm{L}} = g^\star_{l,\mathrm{R}} = 0$ and a DIRICHLET condition on the left side:

$$c^\star_m \frac{\partial u}{\partial t^\star} = \frac{\partial}{\partial x^\star}\left(d^\star_m \frac{\partial u}{\partial x^\star}\right), \qquad t^\star > 0, \quad x^\star \in \left[0, 1\right], \tag{B.1a}$$

$$u = u_{\mathrm{L}}, \qquad t^\star > 0, \quad x^\star = 0, \tag{B.1b}$$

$$-\, d^\star_m \frac{\partial u}{\partial x^\star} = \mathrm{Bi}_{v,\mathrm{R}} \cdot \left(u - u_{\mathrm{R}}(t^\star)\right), \qquad t^\star > 0, \quad x^\star = 1, \tag{B.1c}$$

$$u = 1, \qquad t^\star = 0, \quad x^\star \in \left[0, 1\right]. \tag{B.1d}$$

The dimensionless properties of the material are $d^\star_m = 1$ and $c^\star_m = 430$. The reference time is $t^0 = 1$ h, thus the final simulation time is fixed to $t^\star = 120$. The BIOT number

is $\mathrm{Bi}_{v,\mathrm{R}} = 333$. The boundary conditions are expressed as:

$$u_{\mathrm{L}} = 1\,,$$
$$u_{\mathrm{R}}(t^\star) = 1 + 1.6\,\sin^2\left(\frac{2\pi\,t^\star}{48}\right).$$

B.2. Parametric case

Problem (2.4) is taken into account with $g^\star_{l,\mathrm{L}} = g^\star_{l,\mathrm{R}} = 0$ and a DIRICHLET condition on the left side, the same as in the previous case. The reference time is $t^0 = 1\ \mathsf{h}$, thus the final simulation time is fixed to $t^\star = 120$. The BIOT number is $\mathrm{Bi}_{v,\mathrm{R}} = 100$. The boundary conditions are expressed as:

$$u_{\mathrm{L}} = 1\,,$$
$$u_{\mathrm{R}}(t^\star) = 1 + 1.6\,\sin^2\left(\frac{2\pi\,t^\star}{48}\right).$$

The dimensionless properties of the materials are $d^\star_m = 1$ and $c^\star_m$ assume the following values:

i	1	2	3	4	5	6	7	8	9	10
$c^\star_{m,i}$	833	576	441	357	300	258	227	203	183	166

B.3. Nonlinear case

Problem (2.4) is taken into account with $g^\star_{l,\mathrm{L}} = g^\star_{l,\mathrm{R}} = 0$ and ROBIN condition on both boundaries. The BIOT number are $\mathrm{Bi}_{v,\mathrm{L}} = 10$ and $\mathrm{Bi}_{v,\mathrm{R}} = 15$. The boundary conditions are expressed as:

$$u_{\mathrm{L}}(t^\star) = 1 + 0.3\left[1 - \cos\left(\frac{2\pi\,t^\star}{24}\right)\right],$$
$$u_{\mathrm{R}}(t^\star) = 1 + 0.6\,\sin^2\left(\frac{2\pi\,t^\star}{60}\right).$$

The reference time is $t^0 = 1\ \mathsf{h}$, thus the final simulation time is fixed to $t^\star = 120$. The dimensionless properties of the materials are:

$$d^\star_m(u) = \left(0.86 + 0.25\,u\right)\cdot 5\cdot 10^{-3},$$
$$c^\star_m(u) = 3.36 - 6.11\,u + 3.37\,u^2.$$

References

[1] M. Abuku, H. Janssen, and S. Roels. Impact of wind-driven rain on historic brick wall buildings in a moderately cold and humid climate: Numerical analyses of mould growth risk, indoor climate and energy consumption. *Energy and Buildings*, 41(1):101–110, jan 2009. 5

[2] J. V. Aguado, F. Chinesta, A. Leygue, E. Cueto Prendes, and A. Huerta. Deim-based PGD for parametric nonlinear model order reduction. In *International Conference on Adaptive Modeling and Simulation*, pages 29–34. Centre Internacional de Mètodes Numèrics en Enginyeria (CIMNE), 2013. 24

[3] S. A. Al-Sanea and M. F. Zedan. Improving thermal performance of building walls by optimizing insulation layer distribution and thickness for same thermal mass. *Applied Energy*, 88(9):3113–3124, sep 2011. 15

[4] S. A. Al-Sanea, M. F. Zedan, and S. A. Al-Ajlan. Effect of electricity tariff on the optimum insulation-thickness in building walls as determined by a dynamic heat-transfer model. *Applied Energy*, 82(4):313–330, dec 2005. 15

[5] A. Ammar and F. Chinesta. Circumventing Curse of Dimensionality in the Solution of Highly Multidimensional Models Encountered in Quantum Mechanics Using Meshfree Finite Sums Decomposition. In *Meshfree Methods for Partial Differential Equations IV*, pages 1–17. Springer Berlin Heidelberg, Berlin, Heidelberg, 2008. 11

[6] A. Ammar, B. Mokdad, F. Chinesta, and R. Keunings. A new family of solvers for some classes of multidimensional partial differential equations encountered in kinetic theory modelling of complex fluids. *J. Non-Newtonian Fluid Mech.*, 144(2-3):98–121, jul 2007. 11

[7] A. Ammar, M. Normandin, F. Daim, D. Gonzalez, E. Cueto, and F. Chinesta. Non incremental strategies based on separated representations: applications in computational rheology. *Comm. Math. Sci.*, 8(3):671–695, 2010. 11

[8] N. Aste, A. Angelotti, and M. Buzzetti. The influence of the external walls thermal inertia on the energy performance of well insulated buildings. *Energy and Buildings*, 41(11):1181–1187, nov 2009. 16

[9] I. Axaopoulos, P. Axaopoulos, and J. Gelegenis. Optimum insulation thickness for external walls on different orientations considering the speed and direction of the wind. *Applied Energy*, 117:167–175, mar 2014. 15

[10] B. Bauklimatik Dresden. Simulation program for the calculation of coupled heat, moisture, air, pollutant, and salt transport. *http://www.bauklimatik-dresden.de/delphin/index.php?aLa=en*, 2011. 5

[11] T. Bednar and C.-E. Hagentoft. Analytical solution for moisture buffering effect Validation exercises for simulation tools. In *7th Nordic Symposium on Building Physics*, Reykjavik, Iceland, 2005. 13

[12] J. Berger and N. Mendes. An innovative method for the design of high energy performance building envelopes. *Applied Energy*, 190:266–277, mar 2017. 19

[13] J. Berger, N. Mendes, S. Guernouti, M. Woloszyn, and F. Chinesta. Review of Reduced Order Models for Heat and Moisture Transfer in Building Physics with Emphasis in PGD Approaches. *Archives of Computational Methods in Engineering*, pages 1–13, jul 2016. 5, 11

[14] B. Bognet, F. Bordeu, F. Chinesta, A. Leygue, and A. Poitou. Advanced simulation of models defined in plate geometries: 3D solutions with 2D computational complexity. *Comp.*

Meth. Appl. Mech. Eng., 201-204:1–12, jan 2012. 11

[15] D. E. M. Bond, W. W. Clark, and M. Kimber. Configuring wall layers for improved insulation performance. *Applied Energy*, 112:235–245, dec 2013. 15

[16] J. P. Boyd. *Chebyshev and Fourier Spectral Methods*. New York, 2nd edition, 2000. 8, 9

[17] C. Canuto, M. Y. Hussaini, A. Quarteroni, and T. A. Zang. *Spectral Methods Fundamentals in Single Domains*. Scientific Computation. Springer-Verlag Berlin Heidelberg, 2006. 10

[18] S. Chaturantabut and D. C. Sorensen. Nonlinear Model Reduction via Discrete Empirical Interpolation. *SIAM J. Sci. Comput.*, 32(5):2737–2764, jan 2010. 24

[19] F. Chinesta, A. Ammar, A. Leygue, and R. Keunings. An overview of the proper generalized decomposition with applications in computational rheology. *J. Non-Newtonian Fluid Mech.*, 166(11):578–592, jun 2011. 19

[20] F. Chinesta, R. Keunings, and A. Leygue. *The Proper Generalized Decomposition for Advanced Numerical Simulations: A Primer*. Springer International Publishing, New York, 2013. 11

[21] F. Chinesta, P. Ladevèze, and E. Cueto. A Short Review on Model Order Reduction Based on Proper Generalized Decomposition. *Archives of Computational Methods in Engineering*, 18(4):395–404, nov 2011. 11, 19

[22] F. Chinesta, A. Leygue, F. Bordeu, J. V. Aguado, E. Cueto, D. Gonzalez, I. Alfaro, A. Ammar, and A. Huerta. PGD-Based Computational Vademecum for Efficient Design, Optimization and Control. *Archives of Computational Methods in Engineering*, 20(1):31–59, mar 2013. 11

[23] A. Dalgliesh, S. Cornick, W. Maref, and P. Mukhopadhyaya. Hygrothermal Performance of Building Envelopes: Uses for 2D and 1D simulation. In *10th Conference on Building Science and Technology*, Ottawa, Canada, 2005. NRC Publication Archive. 5

[24] G. H. Dos Santos and N. Mendes. Simultaneous heat and moisture transfer in soils combined with building simulation. *Energy and Buildings*, 38(4):303–314, 2006. 5

[25] T. A. Driscoll, N. Hale, and L. N. Trefethen. Chebfun Guide. *Pafnuty Publications*, Oxford, 2014. 14

[26] A. Dumon, C. Allery, and A. Ammar. Proper general decomposition (PGD) for the resolution of Navier-Stokes equations. *J. Comp. Phys.*, 230(4):1387–1407, 2011. 11

[27] I. Fraunhofer. Wufi. *http://www.hoki.ibp.fhg.de/wufi/wufi_frame_e.html*, 2005. 5

[28] S. Gasparin, J. Berger, D. Dutykh, and N. Mendes. Spectral Methods - Part 1: A fast and accurate approach for solving nonlinear diffusive problems. *Submitted*, pages 1–30, 2017. 5, 9, 10, 14, 24

[29] S. Gasparin, J. Berger, D. Dutykh, and N. Mendes. Stable explicit schemes for simulation of nonlinear moisture transfer in porous materials. *J. Building Perf. Simul.*, pages 1–21, 2017. 5, 7, 20, 26

[30] W. Gautschi. *Orthogonal Polynomials: Computation and Approximation*. Oxford University Press, Oxford, UK, 2004. 9

[31] M. Girault, S. Derouineau, J. Salat, and D. Petit. Réduction de modèle en convection naturelle par une méthode d'identification. *C. R. Mécanique*, 332(10):811–818, 2004. 5

[32] M. Girault and D. Petit. Identification methods in nonlinear heat conduction. Part I: Model reduction. *Int. J. Heat Mass Transfer*, 48(1):105–118, 2005. 5

[33] G. Golub and C. Van Loan. *Matrix Computations*. J. Hopkins University Press, 3rd ed. edition, 1996. 24

[34] M. Ibrahim, P. H. Biwole, P. Achard, E. Wurtz, and G. Ansart. Building envelope with a new aerogel-based insulating rendering: Experimental and numerical study, cost analysis, and thickness optimization. *Applied Energy*, 159:490–501, dec 2015. 15

[35] H. Janssen. Simulation efficiency and accuracy of different moisture transfer potentials. *J. Building Perf. Simul.*, 7(5):379–389, sep 2014. 5, 6

[36] H. Janssen, B. Blocken, and J. Carmeliet. Conservative modelling of the moisture and heat transfer in building components under atmospheric excitation. *Int. J. Heat Mass Transfer*, 50(5-6):1128–1140, mar 2007. 5

[37] M. Labat, C. Magniont, N. Oudhof, and J.-E. Aubert. From the experimental characterization of the hygrothermal properties of straw-clay mixtures to the numerical assessment of their buffering potential. *Building and Environment*, 97:69–81, feb 2016. 16

[38] P. Ladevèze. Sur une famille d'algorithmes en mécanique des structures. *Comptes-rendus des séances de l'Académie des sciences. Série 2, Mécanique-physique, chimie, sciences de l'univers, sciences de la terre*, 300(2):41–44, 1985. 11

[39] H. Lamari, A. Ammar, A. Leygue, and F. Chinesta. On the solution of the multidimensional Langer's equation using the proper generalized decomposition method for modeling phase transitions. *Modelling and Simulation in Materials Science and Engineering*, 20(1):7–15, jan 2012. 11

[40] N. Mendes, M. Chhay, J. Berger, and D. Dutykh. *Numerical methods for diffusion phenomena in building physics*. PUCPRess, Curitiba, Parana, 2017. 9

[41] N. Mendes and P. C. Philippi. A method for predicting heat and moisture transfer through multilayered walls based on temperature and moisture content gradients. *Int. J. Heat Mass Transfer*, 48(1):37–51, 2005. 5

[42] L. H. Mortensen, M. Woloszyn, C. Rode, and R. Peuhkuri. Investigation of Microclimate by CFD Modeling of Moisture Interactions between Air and Constructions. *J. Building Phys.*, 30(4):279–315, apr 2007. 5

[43] D. Néron and P. Ladevèze. Proper Generalized Decomposition for Multiscale and Multiphysics Problems. *Arch. Comp. Meth. Eng.*, 17(4):351–372, dec 2010. 11

[44] S. Niroomandi, I. Alfaro, E. Cueto, and F. Chinesta. Accounting for large deformations in real-time simulations of soft tissues based on reduced-order models. *Computer Methods and Programs in Biomedicine*, 105(1):1–12, jan 2012. 11

[45] A. Nouy. A generalized spectral decomposition technique to solve a class of linear stochastic partial differential equations. *Comp. Meth. Appl. Mech. Eng.*, 196(45-48):4521–4537, sep 2007. 11

[46] M. Ozel. Effect of wall orientation on the optimum insulation thickness by using a dynamic method. *Applied Energy*, 88(7):2429–2435, jul 2011. 15

[47] M. N. Ozisik. *Heat conduction*. Wiley-Interscience, New York, 2 edition, 1993. 14

[48] E. Palomo del Barrio, S. Raji, M. Duquesne, and A. Sempey. Reduced models for coupled heat and moisture transfer simulation in wood walls. *JP Journal of Heat and Mass Transfer*, 10(1):1–32, 2014. 5

[49] D. Petit, R. Hachette, and D. Veyret. A Modal Identification Method To Reduce A High-Order Model: Application To Heat Conduction Modelling. *Int. J. Model. Sim.*, 17(4):242–250, 1997. 5

[50] R. Peyret. *Spectral methods for incompressible viscous flow*. Springer-Verlag, New York, 2002. 9, 10

[51] E. Pruliere, F. Chinesta, and A. Ammar. On the deterministic solution of multidimensional parametric models using the Proper Generalized Decomposition. *Math. Comp. Simul.*, 81(4):791–810, dec 2010. 11

[52] H. Rafidiarison, R. Rémond, and E. Mougel. Dataset for validating 1-D heat and mass transfer models within building walls with hygroscopic materials. *Building and Environment*, 89:356–368, jul 2015. 24

[53] C. Rode and R. H. Peuhkur. The Concept of Moisture Buffer Value of Building Materials and its Application in Building Design. In *Healthy Buildings 2006*, pages 57–62. 2006. 13, 19

[54] S. Rouchier, M. Woloszyn, G. Foray, and J.-J. Roux. Influence of concrete fracture on the rain infiltration and thermal performance of building facades. *Int. J. Heat Mass Transfer*, 61:340–352, jun 2013. 5

[55] L. F. Shampine and M. W. Reichelt. The MATLAB ODE Suite. *SIAM J. Sci. Comput.*, 18:1–22, 1997. 14

[56] H.-J. Steeman, M. Van Belleghem, A. Janssens, and M. De Paepe. Coupled simulation of heat and moisture transport in air and porous materials for the assessment of moisture related damage. *Building and Environment*, 44(10):2176–2184, oct 2009. 5

[57] L. N. Trefethen. *Finite Difference and Spectral Methods for Ordinary and Partial Differential Equations*. Unpublished, Ithaca, NY, USA, 1996. 8

[58] M. Woloszyn and C. Rode. Tools for performance simulation of heat, air and moisture conditions of whole buildings. *Building Simulation*, 1(1):5–24, mar 2008. 5

[59] J. Yuan, C. Farnham, K. Emura, and M. A. Alam. Proposal for optimum combination of reflectivity and insulation thickness of building exterior walls for annual thermal load in Japan. *Building and Environment*, 103:228–237, jul 2016. 15

S. Gasparin: LAMA, UMR 5127 CNRS, Université Savoie Mont Blanc, Campus Scientifique, F-73376 Le Bourget-du-Lac Cedex, France and Thermal Systems Laboratory, Mechanical Engineering Graduate Program, Pontifical Catholic University of Paraná, Rua Imaculada Conceição, 1155, CEP: 80215-901, Curitiba – Paraná, Brazil
E-mail address: suelengasparin@hotmail.com
URL: https://www.researchgate.net/profile/Suelen_Gasparin/

J. Berger: LOCIE, UMR 5271 CNRS, Université Savoie Mont Blanc, Campus Scientifique, F-73376 Le Bourget-du-Lac Cedex, France
E-mail address: Berger.Julien@univ-smb.fr
URL: https://www.researchgate.net/profile/Julien_Berger3/

D. Dutykh: LAMA, UMR 5127 CNRS, Université Savoie Mont Blanc, Campus Scientifique, F-73376 Le Bourget-du-Lac Cedex, France
E-mail address: Denys.Dutykh@univ-smb.fr
URL: http://www.denys-dutykh.com/

N. Mendes: Thermal Systems Laboratory, Mechanical Engineering Graduate Program, Pontifical Catholic University of Paraná, Rua Imaculada Conceição, 1155, CEP: 80215-901, Curitiba – Paraná, Brazil
E-mail address: Nathan.Mendes@pucpr.edu.br
URL: https://www.researchgate.net/profile/Nathan_Mendes/